

# Investigation of biocide efficacy by photoacoustic biofilm monitoring

T. Schmid<sup>a</sup>, U. Panne<sup>a,\*</sup>, J. Adams<sup>b</sup>, R. Niessner<sup>a</sup>

<sup>a</sup>*Institute of Hydrochemistry, Technical University of Munich, Marchioninstr. 17, 81377 Munich, Germany*

<sup>b</sup>*Bernd Schwegmann GmbH & Co. KG, Grafenschaft-Gelsdorf, Germany*

Received 22 May 2003; received in revised form 26 September 2003; accepted 1 October 2003

## Abstract

The undesired growth of biofilms on solid surfaces is often termed biofouling. Biofilms consist mainly of water and microbial cells which are embedded in a biopolymer matrix. Biofouling lowers the water quality and increases the frictional resistance in tubes. Further, biofilms increase the pressure differences in membrane processes and can clog filtration membranes, valves, and nozzles. For investigation and improvement of biocide efficacy and anti-fouling strategies, on-line and in situ monitoring of the biofilm is necessary. In this study, photoacoustic spectroscopy (PAS) was employed for biofilm monitoring. PAS allows the depth-resolved investigation of growth and detachment processes of biofilms. Strategies based on the oxidant hydrogen peroxide were compared to popular isothiazolinone biocides. Hydrogen peroxide allowed a very fast and efficient removal of attached biofilms, whereas no effect on the biofilm matrix was observed in most cases when isothiazolinone biocides were used.

© 2003 Elsevier Ltd. All rights reserved.

*Keywords:* Biofouling; Biocide efficacy; Biofilm monitoring; Photoacoustic spectroscopy; Hydrogen peroxide; Isothiazolinone

## 1. Introduction

The undesired deposition of biological material on solid surfaces is termed biofouling [1]. Microbial biofouling is caused by biofilms, which are layers of microorganisms embedded in a matrix of extracellular polymer substances (EPS) [2]. Life inside an EPS matrix offers many advantages for bacteria and protozoa. The cells can form microconsortia with relatively high mechanical stability and high cell density in which the degradation of complex substrates can be performed orchestrated and synergistically. The EPS matrix can absorb nutrients and is a protective barrier against biocides, changes of the physico-chemical conditions, phagocytosis, and some predator species [1]. Biofouling can occur in almost every technical system under extremely diverse conditions, even in space stations [3].

Biofilm growth on heat exchangers can seriously decrease the heat transfer efficiency [4]. Biofouling increases the frictional resistance in tubes and on ship hulls. Biofilm flocs which are detached from tube surfaces can clog tubes, valves, and nozzles. In membrane processes, biofilms increase the pressure differences and can lead to membrane clogging [5]. Due to the decrease in water quality, biofouling must be controlled in drinking-water reservoirs and distribution systems as well as in food processing systems [6,7]. Additionally, biofilms can provide a habitat for pathogenic microorganisms [8].

For investigation and improvement of biocide efficacy and anti-fouling strategies, on-line and in situ monitoring of biofilms is necessary. For nondestructive monitoring of biofilms, spectroscopic techniques based on light absorption and scattering are used [9,10]. For example, fiber optical sensor devices (FOS) can detect the light which is backscattered by biofilms growing on the tip of an optical fiber [1]. Fluorescence and FTIR-ATR spectroscopy provide a more specific detection of

\*Corresponding author. Tel.: +49-89-2180-7842; fax: +49-89-2180-78255.

E-mail address: ulrich.panne@ch.tum.de (U. Panne).

biological depositions [11–14]. An example for a non-spectroscopic technique for biofilm monitoring is a quartz crystal microbalance (QMB) [15]. In this study, a biofilm monitoring technique was used which is based on photoacoustic spectroscopy (PAS). PAS combines features of optical spectroscopy and ultrasonic tomography and allows—in contrast to other spectroscopic techniques—a depth-resolved analysis of both optically and acoustically inhomogeneous media. Additionally, PAS allows optical absorption measurements even in strongly scattering or optical opaque media. A comparison of PAS to the properties of other biofilm monitoring techniques is given in [16].

### 1.1. Photoacoustic spectroscopy

Photoacoustic spectroscopy is based on the absorption of electromagnetic radiation inside a sample. Via non-radiative relaxation of excited molecules, the absorbed energy is converted into heat. Due to the thermal expansion of the medium, pressure waves are generated which can be detected by microphones or piezoelectric transducers [17]. If short laser pulses are used for excitation, ultrasonic shock waves are generated inside condensed matter. The amplitude  $p$  of a shock wave can be generally described by

$$p \propto \frac{\beta c^2}{C_p} E_0 \mu_a, \quad (1)$$

where  $\beta$  is the thermal expansion coefficient,  $c$  is the speed of sound,  $C_p$  is the heat capacity,  $E_0$  is the pulse energy, and  $\mu_a$  is the absorption coefficient of the sample [18]. For samples consisting predominantly of water (e.g. aqueous solutions and biological matrices), the physical properties of water ( $c = 1490 \text{ m s}^{-1}$ ) can be assumed. The temperature dependence of  $C_p$ ,  $\beta$ , and  $c$  can be corrected by use of literature data as demonstrated in [19]. After normalization to the laser pulse energy, optical absorption coefficients can be derived from the measured pressure amplitudes.

The time delay  $t$  between laser pulse and pressure detection depends on the distance  $z$  between absorbing object and detector:

$$z = ct. \quad (2)$$

Therefore, a time-resolved detection of laser-induced pressure waves permits a depth-resolved investigation of layered samples [20].

Earlier studies revealed the potential of PAS for on-line and in situ monitoring of biofilm growth, detachment, and thickness [21,22]. For excitation of photoacoustic signals at a wavelength of 532 nm, a frequency-doubled Nd:YAG laser was used. Electromagnetic radiation in the visible spectral range is absorbed by pigments inside the microbial cells and in the EPS matrix. The signal amplitude reflects therefore the

density of the immobilized biomass. Independently from this, the thickness of the biofilm can be recorded by depth-resolved measurements. The position of the minimum of the photoacoustic signal reflects the interface region between biofilm and bulk liquid phase. This possibility for biofilm thickness measurements was verified with biofilm models with known thickness and with real biofilms using confocal laser scanning microscopy (CLSM) as independent method. These investigations revealed that the speed of sound in biofilm models consisting of Agar–Agar hydrogel and in real biofilms is approximately equal to the sound velocity in water. Deviations from this value are smaller than the temporal resolution of the piezoelectric detector [21].

Earlier studies were devoted to interactions between biofilms and soluble compounds (e.g. acids or bases) [21,22] as well as particulate matter [16,21]. Additionally, the influence of the flow conditions on structure and thickness of biofilms was examined [21]. Here, first investigations with PAS regarding biocide efficacy are presented.

## 2. Materials and methods

### 2.1. Experimental setup

For investigation of biofilms, three photoacoustic sensor heads were integrated into a flow channel (Fig. 1(a)). Biofilms are grown directly on the surfaces of the sensor heads and investigated by photoacoustic measurements. The photoacoustic sensor heads consist of a 25- $\mu\text{m}$ -thick piezoelectric poly(vinylidene fluoride) (PVDF) film which is coupled to a transparent prism by a conductive epoxy (Fig. 1(b)). The properties of the PVDF film determine the depth resolution of the photoacoustic measurements which is approximately 10  $\mu\text{m}$  in samples consisting predominantly of water [21]. Laser pulses with a wavelength of 532 nm were generated by a frequency-doubled Nd:YAG laser (Surelite 10-I, Continuum, Santa Clara, CA) and guided via optical fibers (HCG-MO550T-10, Laser Components, Santa Rosa, CA) to the sensor heads. The biofilm was illuminated through the transparent prism and laser-induced pressure waves were detected by the piezoelectric film. The detector is circular with a diameter of 5 mm, allowing a representative area of 20 mm<sup>2</sup>. The signal was pre-amplified (HCA-100 M-50 k-C current amplifier, Femto Messtechnik, Berlin, Germany) and recorded by a digital storage oscilloscope (TDS 540, Tektronix, Beaverton, OR). Each photoacoustic measurement was averaged over 100 laser pulses. A more detailed description of the experimental setup can be found in [21].

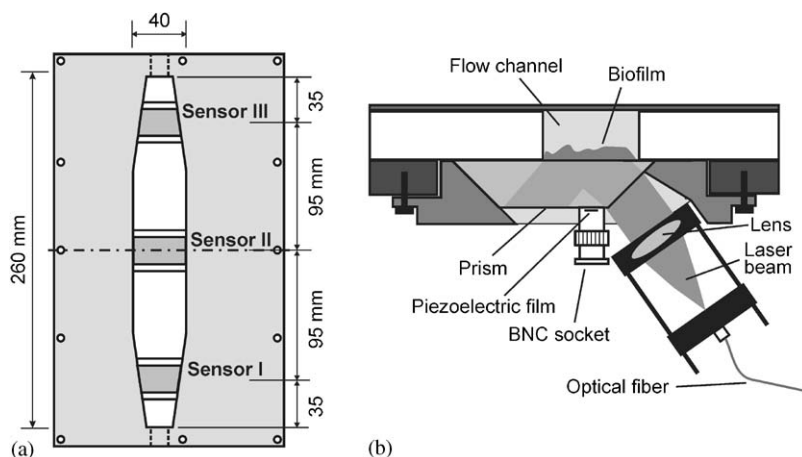


Fig. 1. Flow channel with three integrated photoacoustic sensor heads for investigation of biofilms (a) and cut view through the flow channel at sensor head II (b).

## 2.2. Biocides

The effect of the oxidant hydrogen peroxide (Merck, Darmstadt, Germany) on biofilms was examined in the concentration range from 200 to 1000 ppm. Additionally, hydrogen peroxide was tested in combination with the MOL<sup>®</sup>ox catalyst (MOL<sup>®</sup>CLEAN-technology, MOL Katalysatortechnik GmbH, Merseburg, Germany) which is distributed by Bernd Schwegmann GmbH & Co. KG (Grafschaft-Gelsdorf, Germany) in the area of printing machines [23,24]. The catalyst under study was a 12 × 12-cm wire netting which increases the efficiency of hydrogen peroxide in biofilm removal when it is present inside the bulk liquid.

In comparison to cleaning strategies which are based on hydrogen peroxide, the effect of isothiazolinone biocides was investigated. Isothiazolinones are fast-acting biocides which inhibit growth and metabolism of both algae and bacteria [25]. These biocides are used as single compounds and mixtures of isothiazolinones and other compounds as well. The active component of the commercial product A is 2-octyl-2H-isothiazolin-3-one, product B contains 5-chloro-2-methyl-2H-isothiazolin-3-one, less than 1% 2-methyl-2H-isothiazolin-3-one, and additionally 5–10% 2-bromo-2-nitro-1,3-propanediol, product C contains the same isothiazolinone derivative as product A (2-octyl-2H-isothiazolin-3-one), but the main component (50–100%) of product C is [1,2-ethanediy]bis(oxy)]-bis-methanol. Each isothiazolinone biocide or biocide mixture was used in a concentration of 3%.

## 2.3. Experimental procedure

For generation of biofilms, a mixture of microorganisms taken from an aerobic sequencing batch reactor

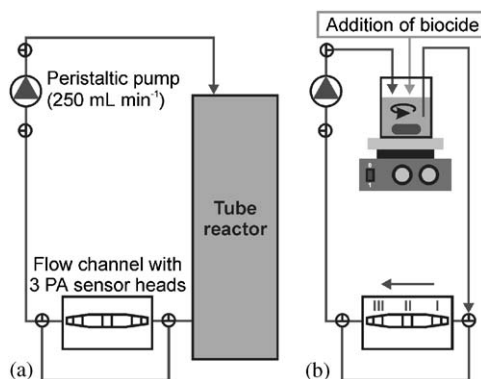


Fig. 2. Experimental procedure for investigation of anti-biofouling strategies: growth of biofilms (a) and addition of a biocide (b).

was grown inside a 18-L tube reactor and fed by a nutrient solution consisting of 690 mg L<sup>-1</sup> sodium acetate, 60 mg L<sup>-1</sup> potassium dihydrogen phosphate, 252 mg L<sup>-1</sup> ammonium sulfate, 19 mg L<sup>-1</sup> potassium chloride, and 4 mg L<sup>-1</sup> yeast extract. In order to achieve aerobic conditions, the reactor was aerated with compressed air with a volume flow of 1 L min<sup>-1</sup>. Within the first part of the experiments, biofilms were generated inside the flow channel. To enhance the adhesion of microbial cells and biopolymers to the sensor heads, the glass surface was modified by an aminoalkyl silane: 1 mL of *N*-(2-aminoethyl)-3-aminopropyl-methyldimethoxy silane was dissolved in a mixture of 10 mL methanol and 10 mL water. The surfaces of the sensor heads were treated with this solution for 12 h at room temperature. Afterwards, the flow channel was flushed with water and the content of the tube reactor was pumped through the channel over 4 h with a volume flow of 250 mL min<sup>-1</sup> (Fig. 2(a)).

To stop the adhesion of biofilm flocs to the sensor heads, the flow channel was disconnected from the tube reactor within the second part of the experiments (Fig. 2(b)). In order to simulate the conditions in a technical process, tap water from a stirred 1-L beaker was circulated through the system with a volume flow of  $250 \text{ mL min}^{-1}$ . After a 20 h equilibration period, the content of the beaker was replaced by fresh tap water in order to prevent reactions of the biocide with soluble or suspended organic compounds. At each sensor head, four photoacoustic measurements were performed as a reference before addition of a biocide. Afterwards, aliquots of hydrogen peroxide or products A, B, and C, respectively, were added in order to achieve  $\text{H}_2\text{O}_2$  concentrations of 200, 600, or 1000 ppm and a concentration of 3% of the isothiazolinone products. Photoacoustic measurements were performed over several hours to monitor changes in biofilm density and structure.

### 3. Results and discussion

#### 3.1. Biofilm detachment by hydrogen peroxide

Fig. 3 exhibits the photoacoustic signal amplitudes at sensor head III after addition of 200, 600, and 1000 ppm hydrogen peroxide. The signal was normalized to its value before biocide addition. As can be seen, the signal amplitude begins to decrease a few minutes after  $\text{H}_2\text{O}_2$  addition and reaches less than 20% of the initial value within 30 min in every experiment. This fast decrease in absorbance cannot be explained simply by bleaching effects due to the oxidant hydrogen peroxide. Significant bleaching of detached biofilm flocs was observed only after repeated additions of hydrogen peroxide aliquots. Thus, decrease in signal intensity is in this case due to the removal of adsorbed biomass. This was verified by

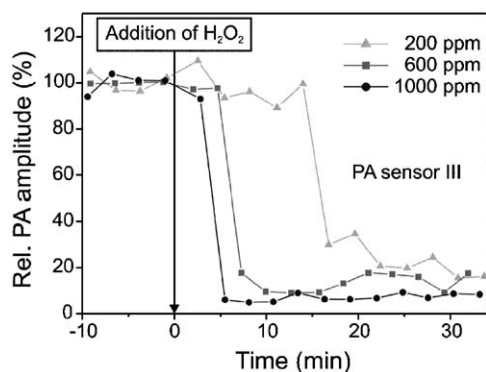


Fig. 3. Photoacoustic signal amplitude at sensor head III after addition of 200, 600, and 1000 ppm hydrogen peroxide, respectively.

depth-resolved measurements and elucidation of the detachment mechanism (see below). Every hydrogen peroxide concentration resulted in a decrease in signal intensity of approximately 80%, but there were significant differences in the detachment rate. In the case of 200 ppm, the decrease of the signal amplitude began at 15 min after  $\text{H}_2\text{O}_2$  addition, whereas biofilm detachment was observed 6 and 4 min after addition of 600 and 1000 ppm  $\text{H}_2\text{O}_2$ , respectively.

Differences in the detachment behavior were also observed between the three monitored positions inside the flow channel. Fig. 4 shows photoacoustic measurements on sensor head I, II, and III after addition of 1000 ppm  $\text{H}_2\text{O}_2$ . The signal amplitude on sensor heads II and III decreased within a few minutes by more than 80%. The detached flocs were circulated with the bulk liquid through the system and some of them adsorbed to sensor head II to form a new biofilm with much lower density leading to an increase of the signal amplitude up to 40% of the initial value. In comparison to the sensor heads II and III, biofilm detachment on sensor I was much slower. Within 70 min, the decrease in signal amplitude was only approximately 15%. These differences are due to different flow conditions inside the flow channel. Former investigations revealed, that the development of a turbulent boundary layer at the inlet of the channel lead to the formation of thin biofilms at sensor I with thicknesses of a few 100  $\mu\text{m}$ . These thin biofilms are relatively stable with regard to changes of process parameters such as pH-value or addition of suspended particles. The flow conditions on sensor head II and III allow the sorption of relatively large biofilm flocs to the solid surface leading to biofilm thicknesses up to 1 mm. The flocs which are adsorbed on the surface of a relatively stable base biofilm, are removed by changes of the pH-value or collision with suspended particles [21]. A similar behavior of the biofilm stability could be observed in the experiment described here, i.e. a relatively stable biofilm on sensor head I in comparison to the biofilms on the other sensor heads.

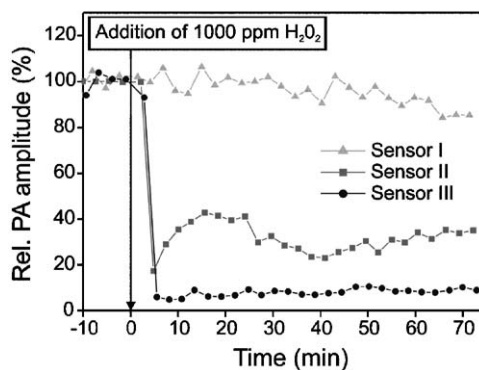


Fig. 4. Photoacoustic signal amplitude at sensor head I, II, and III after addition of 1000 ppm hydrogen peroxide.

In order to examine the effect of the MOL<sup>®</sup>ox catalyst, the experiments with hydrogen peroxide were repeated with the catalyst present in the stirred beaker in form of a wire netting (MOL<sup>®</sup>CLEAN-technology). Fig. 5 reveals photoacoustic measurements at sensor head II after addition of 1000 ppm hydrogen peroxide in presence and absence of the MOL<sup>®</sup>ox catalyst. As can be seen, the detachment rates are very similar. In both cases, the photoacoustic signal amplitude decreased by

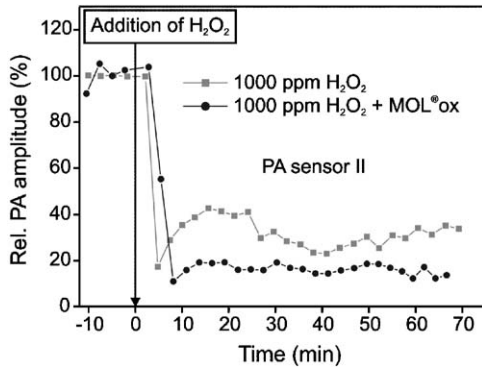


Fig. 5. Comparison of photoacoustic measurements at sensor head II after addition of 1000 ppm hydrogen peroxide in presence and absence of the MOL<sup>®</sup>ox catalyst.

more than 80% within a few minutes. Sorption of detached biofilm flocs to the sensor head led to the formation of a new biofilm in absence of the MOL<sup>®</sup>ox catalyst, whereas the signal was relatively stable after the detachment process, when the catalyst was present in the stirred beaker. Detached flocs interacted with the wire netting and were degraded obviously more efficiently.

Depth-resolved photoacoustic measurements allow the elucidation of the mechanism of the fast detachment process caused by hydrogen peroxide. Fig. 6(a) exhibits photoacoustic signal amplitudes measured at sensor head II after addition of 200 ppm hydrogen peroxide in presence of the MOL<sup>®</sup>ox catalyst. No significant difference in the detachment mechanism was observed between the experiments in presence or absence of the catalyst. Therefore, only one example is given here. The photoacoustic signals are given in the unit of the optical absorption coefficient, i.e. cm<sup>-1</sup>. The penetration depth of photoacoustic measurements is limited by the optical penetration depth, which can be calculated as the reciprocal value of the absorption coefficient. In this case (see Fig. 6 and 8), the optical penetration depth was in the range of 1.5–2.5 mm which is larger than the biofilm thickness. Thus, depth-resolved biofilm measurements were not limited by the penetration depth in this case. The signal began to decrease at 12 min after H<sub>2</sub>O<sub>2</sub>

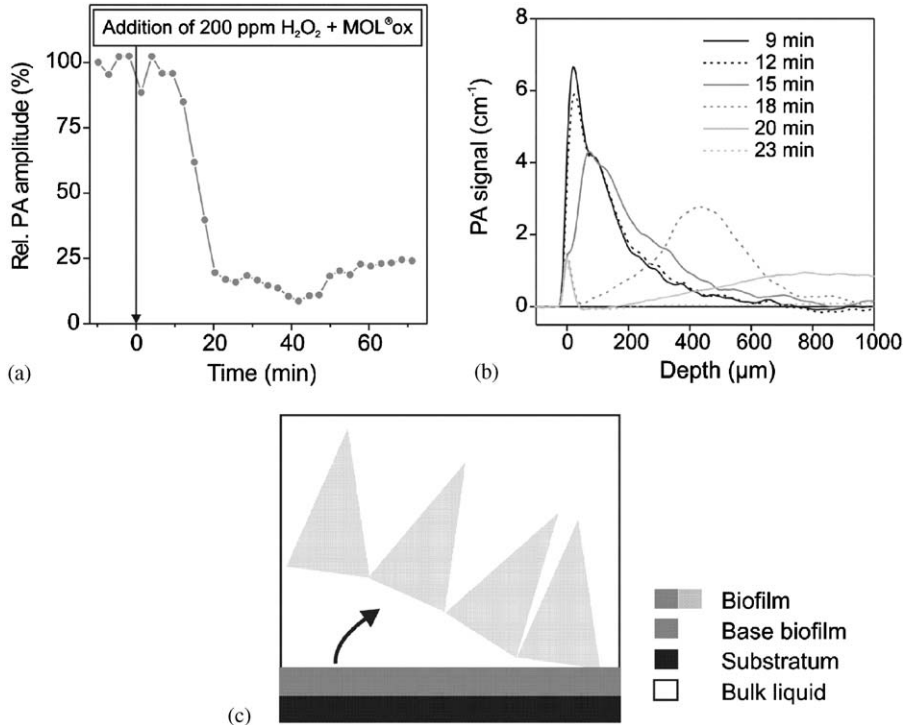


Fig. 6. Elucidation of the mechanism of biofilm detachment caused by 200 ppm hydrogen peroxide in combination with the MOL<sup>®</sup>ox catalyst: photoacoustic amplitudes (a), depth-resolved measurements (b), and schematic representation of the sloughing off mechanism (c).

addition and reached a relatively constant plateau at 23 min (Fig. 6(a)). The corresponding depth-resolved measurements during the detachment process are given in Fig. 6(b). As can be seen, biofilm detachment in this case leads not only to a decrease of the signal amplitude but also to a highly significant change of the shape of the photoacoustic signal. The signal maximum corresponding to the highest absorbance and therefore to the highest biofilm density was at a distance of 24  $\mu\text{m}$  from the solid surface before the beginning of the detachment process. The position of the signal minimum reveals a biofilm thickness of approximately 840  $\mu\text{m}$ . During biofilm detachment, the signal maximum moved to 75  $\mu\text{m}$  at 15 min, 430  $\mu\text{m}$  at 18 min, and 775  $\mu\text{m}$  at 20 min. Finally, the major part of the biofilm was detached from an approximately 60  $\mu\text{m}$  thick base layer of the biofilm which remained on the sensor surface. The thickness of the base layer was estimated by determining the position of the signal minimum on the depth axis which corresponds approximately to the width of the remaining peak in this case. We can conclude that biofilm removal by hydrogen peroxide can be explained by sloughing off of relatively large areas which move towards the bulk liquid phase and are finally detached from the base biofilm (Fig. 6(c)). If bleaching effects would be significant in this case, we would expect a decrease in signal intensity starting at the top and reaching subsequently the base layer of the biofilm reflecting the diffusion of the oxidant inside the biofilm. Due to the shift of signal maximum from the sensor surface towards the bulk liquid, we can conclude that sloughing off is the dominant mechanism and bleaching effects can be neglected.

### 3.2. Effect of isothiazolinone biocides

In contrast to hydrogen peroxide, isothiazolinones inhibit specifically growth and metabolism of microbial cells. Fig. 7 exhibits photoacoustic signal amplitudes measured at sensor head II before and after addition of products A, B, and C which are isothiazolinones as single compound or as mixtures with other organic compounds. Only small and non-significant changes in signal intensity could be observed in this case, when the error bars reflecting the single standard deviation of the measurement are taken into account. Microbial cells are inhibited by isothiazolinones, but the biofilm matrix which is responsible for the major part of the negative effects of biofouling is not affected by them.

Product C which is a mixture of [1,2-ethanediy]bis(oxy)-bis-methanol and 2-octyl-2H-isothiazolin-3-one led to a biofilm detachment on sensor head I. Fig. 8(a) shows the behavior of the photoacoustic signal amplitudes after addition of 3% products A and C, respectively. Product A did not affect the density of the adsorbed biomass. The biofilm removal which was

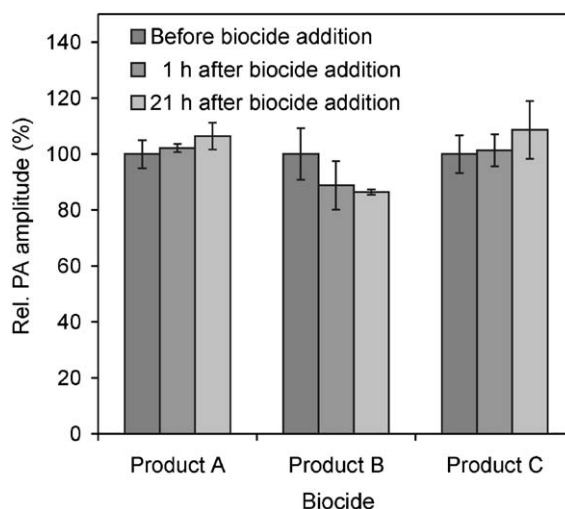


Fig. 7. Photoacoustic amplitudes before and after addition of isothiazolinone biocides.

observed after addition of 3% product C is slower and not as effective as in the case of hydrogen peroxide. Within 50 min, the signal amplitude decreased by approximately 65%. The corresponding depth-resolved measurements (Fig. 8(b)) reveal that the shape of the photoacoustic signal remains constant during the whole detachment process. The minimum of all photoacoustic signals reflecting the interface between biofilm and bulk liquid is at approximately 150  $\mu\text{m}$ . The isothiazolinone component of product C did not affect the biofilm matrix when tested as a single compound (product A). Therefore, [1,2-ethanediy]bis(oxy)-bis-methanol as the major component of product C must be responsible for the biofilm detachment. Product C formed a relatively stable emulsion when it was mixed with water. Probably small biofilm aggregates were detached due to collision with emulsified droplets. The measured biofilm thickness was approximately constant during the whole detachment process. Therefore, it can be concluded that the desorbed flocs are much smaller than the active area of the piezoelectric detector, i.e. 20  $\text{mm}^2$ . Biofilm removal by detachment of microscopic aggregates is commonly termed erosion (Fig. 8(c)).

## 4. Conclusions

The potential of photoacoustic biofilm monitoring in the investigation of the efficacy of diverse biocides has been demonstrated successfully. Monitoring of the photoacoustic signal amplitude in the visible spectral range allows the observation of biofilm detachment caused by biocides. Rate and efficiency of the biofilm removal can be determined. In this way, the effects of different biocides and biocide concentrations can be

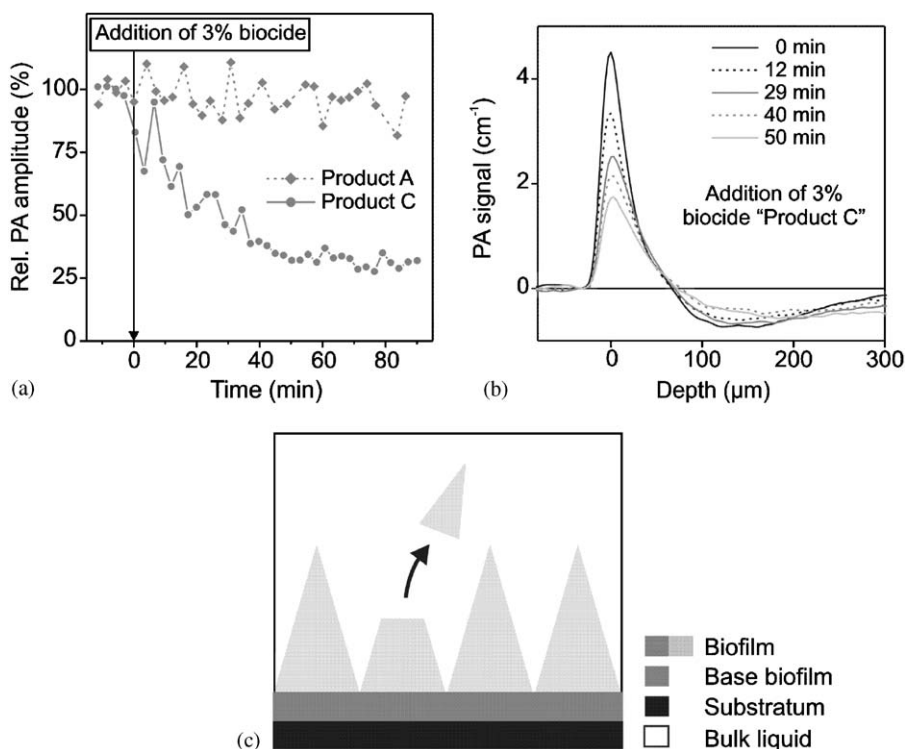


Fig. 8. Elucidation of the mechanism of biofilm detachment caused by 3% product C at sensor head I: photoacoustic amplitudes (a), depth-resolved measurements (b), and schematic representation of biofilm erosion.

compared with each other. Depth-resolved measurements allow the determination of the biofilm thickness and the elucidation of detachment mechanisms.

Hydrogen peroxide reacts as an oxidant with microbial cells and with the biopolymer matrix of biofilms as well. Fast and efficient removal of biofilms was observed even with 200 ppm H<sub>2</sub>O<sub>2</sub> which was the lowest concentration investigated in this study. The fast detachment was caused by sloughing off of relatively large biofilm areas, which moved towards the bulk liquid and desorbed finally from the base layer of the biofilm. Detached biofilm flocs were circulated with the bulk liquid through the system and could adsorb therefore to solid surfaces to form new biofilms with lower density. This biofilm formation after the detachment process could be reduced by use of the MOL<sup>®</sup>ox catalyst in combination with hydrogen peroxide.

In contrast to hydrogen peroxide, isothiazolinone biocides did not affect density and structure of biofilms. Isothiazolinones inhibit specifically growth and metabolism of microbial cells, but do not affect the biopolymer matrix of the biofilm. A mixture of an isothiazolinone and a glycol ether formed a stable emulsion in water and caused a partial biofilm detachment which could be explained by collision of emulsified droplets with biofilm clusters. In this case, the

detachment mechanism was dominated by erosion of microscopical biofilm flocs.

#### Acknowledgements

The authors acknowledge the financial support by Deutsche Forschungsgemeinschaft (DFG) and a grant awarded to Thomas Schmid by Max-Buchner-Forschungsstiftung.

#### References

- [1] Flemming HC. Biofouling in water systems—cases, causes and countermeasures. *Appl Microbiol Biotechnol* 2002;59:629–40.
- [2] Wilderer PA, Characklis WG. Structure and function of biofilms. New York: Wiley; 1989.
- [3] Koenig DW, Pierson DL. Microbiology of the space shuttle water system. *Water Sci Technol* 1997;35: 59–64.
- [4] Melo LF, Bott TR. Biofouling in water systems. *Exp Therm Fluid Sci* 1997;14:375–81.
- [5] Flemming HC. Reverse osmosis membrane biofouling. *Exp Therm Fluid Sci* 1997;14:382–91.

- [6] Percival SL, Knapp JS, Edyvean RGJ, Wales DS. Biofilms, mains water and stainless steel. *Water Res* 1998;32:2187–201.
- [7] Vrouwenvelder HS, van Paassen JAM, Folmer HC, Hofman JAMH, Nederlof MM, van der Kooij D. Biofouling of membranes of drinking water production. *Desalination* 1998;118:157–66.
- [8] Costerton JW, Stewart PS, Greenberg EP. Bacterial biofilms: a common cause of persistent infections. *Science* 1999;284:1318–22.
- [9] Jacobs L, De Bruyn EE, Cloete TE. Spectrophotometric monitoring of biofouling. *Water Sci Technol* 1996;34:533–40.
- [10] Klahre J, Flemming HC. Monitoring of biofouling in papermill process waters. *Water Res* 2000;34:3657–65.
- [11] Kerr A, Cowling MJ, Beveridge CM, Smith MJ, Parr ACS, Head RM, Davenport J, Hodgkiess T. The early stages of marine biofouling and its effect on two types of optical sensors. *Environ Int* 1998;24:331–43.
- [12] Schmitt J, Nivens D, White DC, Flemming HC. Changes of biofilm properties in response to sorbed substances—an FTIR-ATR study. *Water Sci Technol* 1995;32:149–55.
- [13] Suci PA, Vransky JD, Mittelman MW. Investigation of interactions between antimicrobial agents and bacterial biofilms using attenuated total reflection Fourier transform infrared spectroscopy. *Biomaterials* 1998;19:327–39.
- [14] Suci PA, Geesey GG, Tyler BJ. Integration of Raman microscopy, differential interference contrast microscopy, and attenuated total reflection Fourier transform infrared spectroscopy to investigate Chlorohexidine spatial and temporal distribution in *Candida albicans* biofilms. *J Microbiol Methods* 2001;46:193–208.
- [15] Helle H, Vuoriranta P, Välimäki H, Lekkala J, Aaltonen V. Monitoring of biofilm growth with thickness-shear mode quartz resonators in different flow nutrition conditions. *Sensor Actuat B* 2000;71:47–54.
- [16] Schmid T, Panne U, Haisch C, Niessner R. Process analysis of biofilms by photoacoustic spectroscopy. *Anal Bioanal Chem* 2003;375:1124–9.
- [17] Rosencwaig A. Photoacoustics and photoacoustic spectroscopy. New York: Wiley; 1980.
- [18] Tam AC. Applications of photoacoustic sensing techniques. *Rev Mod Phys* 1986;58:381–431.
- [19] Adelhelm K, Faubel W, Ache HJ. Laser-induced photoacoustic spectroscopy in liquid samples: temperature and solvent effects. *Fres J Anal Chem* 1990;338:259–64.
- [20] Karabutov AA, Podymova NB, Letokhov VS. Time-resolved laser photoacoustic tomography of inhomogeneous media. *Appl Phys B* 1996;63:545–63.
- [21] Schmid T, Panne U, Haisch C, Hausner M, Niessner R. A photoacoustic technique for depth-resolved in situ monitoring of biofilms. *Environ Sci Technol* 2002;36:4135–41.
- [22] Schmid T, Panne U, Haisch C, Niessner R. Biofilm monitoring by photoacoustic spectroscopy. *Water Sci Technol* 2003;47:25–9.
- [23] Koppe J, Rappthel I, Lausch H. Process for avoidance of bio fouling. *VGB PowerTechnol* 2002;10:118–20.
- [24] Walter R, Büsching K. Biofilmvermeidung und Biofilmauflösung in Wasserkreisläufen. *WLB Wasser, Luft und Boden* 2002;5:60–6.
- [25] Videla HA. Prevention and control of biocorrosion. *Int Biodeterior Biodegrad* 2002;49:259–70.